Journal of Materials Chemistry A

Accepted Manuscript

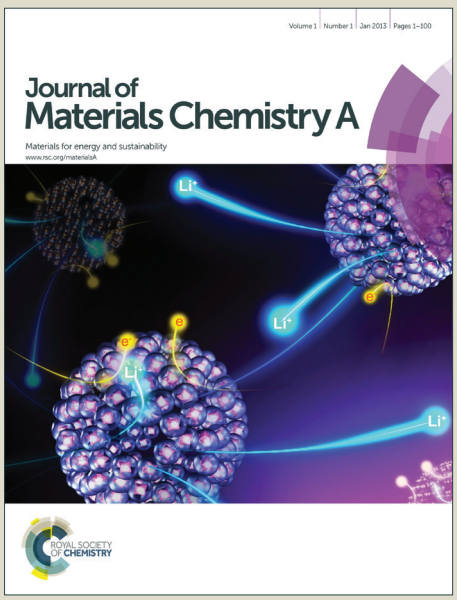

ROYAL SOCIETY OF CHEMISTRY

www.rsc.org/materialsA

Nitrogen-doped reduced graphene oxide for high-performance flexible all-solid-state micro-supercapacitors

Shuangyu Liu,[ab] Jian Xie,[*ac] Haibo Li,[d] Ye Wang,[b] Hui Ying Yang,[*b] Tiejun Zhu,[a] Shichao Zhang,[e] Gaoshao Cao[c] and Xinbing Zhao[ac]

[a]*State Key Laboratory of Silicon Materials, Department of Materials Science and Engineering, Zhejiang University, Hangzhou 310027, China. E-mail: xiejian1977@zju.edu.cn; Fax: +86-571-87951451; Tel: +86-571-87952181*
[b]*Pillar of Engineering Product Development, Singapore University of Technology and Design, 20 Dover Drive, Singapore 138682, Singapore. E-mail: yanghuiying@sutd.edu.sg; Tel: +65 63036663*
[c]*Key Laboratory of Advanced Materials and Applications for Batteries of Zhejiang Province, China*
[d]*Key Laboratory of Ningxia for Photovoltaic Materials, Ningxia University, Yinchuan 750021, China*
[e]*School of Materials Science and Engineering, Beijing University of Aeronautics and Astronautics, Beijing 100191, China*
† Electronic supplementary information (ESI) available: Device for screen printing, N_2 absorption/desorption isotherms of N-doped rGO, cross-sectional SEM image of a MSC, charge and discharge curves of MSC using undoped rGO, self-discharge curve of MSCs, and comparison of specific capacitance of MSCs using graphene materials. See DOI:

Abstract

The rapid development on microelectronic devices has stimulated an increasing demand for micro energy storage devices, typically, micro-supercapacitors (MSCs). Despite recent advances, a challenge still remains to fabricate MSCs with a facile, scalable and inexpensive method. In this work, we use a facile screen printing technique to fabricate flexible all-solid-state MSCs using N-doped reduced graphene oxide (rGO) as the electrode material. The effective area of MSCs and thickness of active material are only 0.396 cm^2 and 10 μm, respectively. The MSCs can deliver a high specific areal capacitance of 3.4 mF cm^{-2}, which is among the high values of graphene-based materials for all-solid-state MSCs reported so far. The easy fabrication and good performance make the MSCs promising on-chip energy storage devices.

Introduction

Energy storage has become a key technological challenge in the 21st century. Electrochemical capacitors, also called supercapacitors or ultracapacitors, recently have received an increasing interest as energy storage devices due to their higher energy density than dielectric capacitors, and longer cycle life, faster charge/discharge rates and higher power density than batteries.[1–5] Compared with supercapacitors with liquid electrolyte, all-solid-state supercapacitors offer many advantages such as light weight, outstanding flexibility and high safety, showing promising applications in flexible, portable electronic devices.[6–12] For instance, an all-solid-state carbon-fiber/MnO_2 based supercapacitor can yield a high specific capacitance of 2.5 F cm^{-3}.[8] The rapid development on miniaturized devices, such as micro-robots, wireless sensors, implantable medical devices and radio frequency identification tags, has stimulated the demand for rechargeable, microscale, and flexible energy storage devices, for example micro-supercapacitors (MSCs).[13] Various materials have been applied for MSCs including carbon materials with electrical-double-layer (EDL) capacitive effect, such as carbon nanotubes (CNT),[14] onion-like carbon,[15] active carbon,[16] graphite,[17] and carbide derived carbon,[18] and conductive polymers and metal oxides with pseudo capacitive effect, such as polypyrrole,[19] polyaniline,[20] MnO_2,[21] and RuO_2.[22]

Compared with pseudo capacitive materials, carbon materials with EDL effect are more practical due to such merits as light weight, high electrical conductivity, large surface area, superior chemical stability, low cost, etc.[23–26] Among various kinds of carbon materials, graphene, a two-dimensional carbon material,[27] has attracted a great attention as electrode material for EDL capacitors[28–31] due to its novel advantages such as large surface area,[28] high electrical conductivity,[32] and huge mechanical strength.[33] Graphene is also attractive for MSCs[30,34–41] because of its appealing physicochemical properties and intrinsic EDL capacitance.[42,43] El Kady et al. reported a novel laser scribed graphene (LSG) microelectrode for MSCs.[35] The MSCs exhibited a high specific capacitance of 3.67 mF cm^{-2} owing to large surface area, abundant open pores and high electronic conductivity of the scribed graphene.[35] Other fabrication methods for graphene-based microelectrodes include spin coating,[39]

electrophoretic deposition,[38,40,41] and layer-by-layer (LBL) assembly.[30] For assembly of MSCs, conventional microelectronic techniques, photolithography, plasma or chemical etching, current collector sputtering, etc., are always involved, making the fabrication process complicated, costly and environmentally unfriendly. Therefore, despite the recent progress, a challenge still remains to fabricate MSCs with a facile, scalable and cost-effective approach.

Herein, we report a simple method based on screen printing to fabricate all-solid-state flexible MSCs using N-doped reduced graphene oxide (rGO) as the electrode material. Compared with conventional microelectronic methods, this method is facile and inexpensive. Screen printing enables electrode deposition and pattering at the same time, considerably reducing the process complexity. In addition, screen printing technology is also compatible with the flexible polymer substrates, for example, polyethylene terephthalate (PET). The single all-solid-state micro-supercapacitor (MSC) can deliver a high specific areal capacitance of 3.4 mF cm^{-2}, which is among the high values of graphene-based materials for all-solid-state MSCs reported to date. The MSCs also exhibit good rate capability and long cycle life. Moreover, the voltage and capacitance can be scaled up by simply connecting the single MSC device in series, parallel or both. The easy fabrication and good performance make the graphene-based MSCs promising applications as on-chip energy storage devices.

Experimental section

Synthesis of N-doped rGO

The synthesis of N-doped rGO was divided into three steps. The first step is to synthesize partially reduced graphene oxide (P-rGO). In a typical procedure, graphite oxide (GO), prepared by a modified Hummers method,[44] was sufficiently dispersed into 0.2 M KOH aqueous solution (200 mL). The pH was adjusted to 9 with Na_2CO_3 aqueous solution. The mixed solution was then heated at 80 ^oC for 2 h under magnetic stirring. P-rGO was obtained after centrifuging at 8000 rpm and rinsing with deionized (DI) water for several times. The P-rGO was then dispersed in 200 mL DI water under vigorous stirring to form solution A. In the second step, 230 mg sulfanilic acid, 90 mg sodium nitrate, and 2 g

HCl (1 M) were mixed in 50 mL DI water to form solution B. Solution B was then added to solution A and reacted in an ice bath for 2 h with constant stirring, resulting in the formation of the intermediate, N-doped P-rGO. In the final step, N-doped P-rGO was re-dispersed in 200 mL DI water followed by adding 5 g hydrazine and reacting at 100 ^{o}C for 24 h under stirring. After rinsing with DI water thoroughly, the final product, N-doped rGO was obtained by filtrating through a vacuum filtration system. Bare rGO was also prepared by a similar route without the step of reaction with sulfanilic acid.

Materials characterization

X-ray photoelectron spectra (XPS) measurements were conducted on a KRATOS AXIS ULTRA-DLD spectrometer with a monochromatic Al K_α radiation ($h\upsilon$ = 1486.6 eV). Morphology of the product was observed by field-emission scanning electron microscopy (SEM) on an FEI-sirion microscope and transmission electron microscopy (TEM) and high-resolution TEM (HRTEM) on a JEM 2100F microscope. N_2 absorption/desorption isotherms were recorded on a Quantachrome Autosorb-1 analyser.

Fabrication and electrochemical measurements of all-solid-state MSCs

The screen printing device includes brush, screen and screen fixer (See Fig. S1 in ESI†). First, brush and screen were used to paint conductive silver paste (SPI Supplies, USA) onto PET substrate (2.5 cm×7.5 cm×220 μm) as the current collector. The silver paste painted on PET was then heated under vacuum at 200 ^{o}C for 1 h to remove the polymer in the silver paste. Second, a slurry composed of N-doped rGO and polyvinylidene fluoride (4:1 in weight) was screen printed onto silver current collector and dried at 110 ^{o}C under vacuum overnight. Finally, gel electrolyte of polyvinyl alcohol (PVA)/H_3PO_4 (1:1 in weight) dispersed in DI water was dropped onto the PET substrate followed by drying naturally in air. The gel electrolyte was made by mixing 3 g PVA and 3 g H_3PO4 in 30 mL DI water and stirring at 80 ºC for 1 h until the solution became transparent. The effective area of a single device is 0.396 cm^2 and the thickness of the printed N-doped rGO layer is around 10 μm. The electrochemical properties of the MSCs were evaluated by galvanostatic charge and discharge cycling at 20–500 μA cm^{-2} and cyclic voltammetry (CV) scanning at 5–100 mV s^{-1} on an electrochemical

workstation (VMP3, Biologic).

Results and discussion

Fig. 1a shows the SEM image of the N-doped rGO with a lateral size of several microns. The wrinkles and transparent feature indicate that the N-doped rGO is rather thin composed probably of few-layered sheets. TEM image in Fig. 1b also shows that the N-doped rGO has a sheet-like structure with a size of several microns. A folded area of the sheet is further characterized by high-resolution TEM (HRTEM) shown in Fig. 1c. The HRTEM image confirms the few-layered feature of N-doped rGO, consistent with the SEM observation. It suggests that functionalization of graphene oxide by sulfanilic acid effectively refrains the restacking of rGO sheets after reduction. This endows N-doped rGO with a high Brunauer-Emmett-Teller (BET) specific surface area (S_{BET}) of 431 m^2g^{-1} while the undoped rGO has a S_{BET} of only 258 m^2g^{-1}. Fig. 1d gives energy dispersive X-ray spectroscopy (EDS) mapping of N-doped rGO, where the uniform distribution of nitrogen element is evident.

XPS was measured to examine the reduction state of GO and the bonding configuration of N atoms in N-doped rGO. Fig. 2a shows the C1s XPS of GO prepared by the modified Hummers method. The spectra can be fitted into four peaks for carbon atoms in different forms: sp^2-hybridized graphitic carbon (C=C, 284.8 eV), carbon in C–O bonds (286.3 eV), carbonyl carbon (C=O, 287.6 eV) and carboxyl carbon (O–C=O, 289. 0 eV).[45] The peak intensity of the oxygenated carbons shows a significant decrease after hydrothermal reaction, indicating a sufficient reduction of GO (Fig. 2b). Two small peaks at 285.8 and 287.6 eV in Fig. 2b are attributed to the formation of C=N bond and C-N bond, respectively.[46] The N atomic percentage in N-doped rGO is estimated to be 4.7% based on the XPS analysis. To further clarify the bonding configuration of N atoms in N-doped rGO, N1s spectra were also measured as shown in Fig. 2c. It is deconvoluted to three peaks that are assigned to pyridinic N (N1: 398.3 eV), pyrrolic N (N2: 399.6 eV), and graphitic N (N3: 400.9 eV).[47,48] As seen in Fig. 2d, the pyridinic N bonds with two C atoms with one p-electron localized in π conjugated system and the pyrrolic N with a pair of p-eletrons. Graphitic N represents nitrogen atoms that substitue carbon atoms

within the hexagonal ring in graphene. We should stress that absorption of N-containing compounds on rGO is also highly possible and that the determination of exact configuration of N atoms in rGO is a technically difficult problem. For simplicity, we use "doping" for both the absorption and lattice doping cases.

Flexible all-solid-state MSCs were fabricated through a screen printing method as shown in Fig. 3. The detailed fabrication process is depicted in the Experimental section. Flexible PET with a thickness of 220 μm was used as the substrate. The MSCs were constructed by successive deposition of Ag as current collector, N-doped rGO as active material and PVA/H_3PO_4 as solid electrolyte. The process is facile and inexpensive unlike the case in conventional microelectronic processing method. The obtained devices are small in size (effective area: 0.396 cm^2) and exhibit a flexible feature, which is desirable for micro-device applications. Fig. 3 also gives the detailed size of a single MSC. The cross-sectional SEM image of a MSC is shown in Fig. S2, from which the thicknesses of N-doped rGO and solid electrolyte are measured to be around 10 and 100 μm, respectively.

Galvanostatic charge and discharge cycling and CV scanning were used to evaluate the electrochemical performance of MSCs with N-doped rGO as the electrode material. Fig. 4a shows the charge and discharge curves of a MSC device at various current densities, from which the capacitances are calculated according to the following equations:

$$C=I\Delta t/\Delta E \quad (1)$$

$$C_A = I\Delta t/\Delta EA \quad (2)$$

$$C_V = I\Delta t/\Delta EV \quad (3)$$

where C (F) is the total capacitance, C_A (F cm^{-2}) is specific areal capacitance, C_v (F cm^{-3}) is the specific volumetric capacitance, I (A) is the discharge current, Δt is the discharge time, ΔE is the potential window during discharge after IR drop, and A (cm^2) and V (cm^3) are the effective area and volume of the printed active material. Note that the charge and discharge curves are not symmetric, and much capacity comes from voltage below 0.1 V during the discharge process. The exact reason for this phenomenon is unclear. It suggests that this may be related to sluggish ion diffusion due to the use

of solid electrolyte with a low ionic conductivity. The calculated C_A values of the MSC device are 3.4, 2.4, 1.9, 1.0 and 0.4 mF cm^{-2}, respectively, at 20, 50, 100, 200 and 500 μA cm^{-2}. The device exhibits a high areal capacitance of 3.4 mF cm^{-2} at 20 μA cm^{-2}, corresponding to a C_V value of 3.4 F cm^{-3} at 20 mA cm^{-3}. The value is comparable with that of MSC (3.67 mF cm^{-2}) assembled by the LSG with a much higher surface area (1520 m^{2}g^{-1}).[35] The value is also higher than those of MSCs with other LSG electrodes (0.51–2.32 mF cm^{-2}),[34,36,37] chemically reduced graphene (0.39–0.46 mF cm^{-2}),[30,38] CH_4 plasma reduced graphene (0.08 mF cm^{-2}),[39] and graphene quantum dots (< 0.67 mF cm^{-2}),[40,41] and higher than those of other carbon materials, such as CNT (0.84 mF cm^{-2}),[14] onion-like carbon (0.9 mF cm^{-2}),[14] active carbon (2.1 mF cm^{-2}),[16] graphite (2.3 mF cm^{-2}),[17] and carbide derived carbon (1.5 mF cm^{-2}).[18] The detailed comparison of these data is given in Table S1. For comparison, the electrochemical performance of MSC using undoped rGO was also measured (Fig. S3). The C_A values are 2.0, 1.5, 1.0, 0.6 and 0.15 mF cm^{-2}, respectively, at 20, 50, 100, 200 and 500 μA cm^{-2}. The higher specific capacitance of N-doped rGO compared with the undoped one can be attributed to its high surface area due to the nitrogen doping and surface absorption of N-containing compounds. Note that for the N-doped rGO, its specific surface area of 450 m^{2}g^{-1} is not a high value compared with normal porous carbons. Thus, its relatively high capacitance may be due to the enhanced contact between solid electrolyte and rGO with the formation some bonds bridged by the doped and absorbed N atoms.

Fig. 4b shows the CV plots of a single MSC at various scan rates. The MSC exhibits a quasi rectangular shape at low scan rates. Repeated galvanostatic cycling of the MSC was performed at 100 μA cm^{-2} shown in Fig. 4c. The charge and discharge curves show a triangular shape, typical of EDL capacitive behavior. In addition, the coulombic efficiency of the MSC reaches 97%, which may be due to its relatively low self-discharge rate (See Fig. S4 in ESI†). The cycling stability of the MSC at 100 μA cm^{-2} is presented in Fig. 4d. After 2000 cycles, the device can maintain 98.4% of its initial capacitance, indicating good cycling stability. This can be attributed to the formation of an efficient interpenetrating network between rGO and solid electrolyte, where the solid electrolyte can keep the structural integrity of the microelectrodes.[35] Fig. 4e shows the rate capability of the MSC. The highest

volumetric capacitance of the MSC is 3.4 F cm^{-3} (3.4 mF cm^{-2}) at 20 mA cm^{-3}. At 500 mA cm^{-3}, it can still deliver a capacitance of 0.4 F cm^{-3} (0.4 mF cm^{-2}). The relationship between volumetric power density and energy density is reflected by the Ragone plot as shown in Fig. 4f. The volumetric energy density and power density are calculated following the equations:

$$E_V = C_V \Delta E^2 / 7200 \quad (4)$$

$$P_V = 3600 E_V / \Delta t \quad (5)$$

where E_V (Wh cm^{-3}) is volumetric energy density, P_V (W cm^{-3}) is volumetric power density, and the definitions of C_V, I ΔE, and Δt are same as those in Equation 1–3. The highest E_V value of the MSC is 3.0×10^{-4} Wh cm^{-3} at 0.2 W cm^{-3}, which is comparable with that of the LSG based MSC with solid electrode at a similar power density.[35]

Generally, the energy that a single MSC can store is too low for practical applications. Therefore, MSCs need to be connected in series, in parallel or in a combination of series and parallel to meet the required voltage and capacitance of micro-devices. The CV scanning (50 mV s^{-1}) and charge and discharge cycling (100 μA cm^{-2}) of 4 MSCs connected in parallel are shown in Fig. 5a and b. The inset in Fig. 5a is the equivalent circuit. For comparison, the capacitive performance of a single MSC is also given with the same scan rate and current density. In the parallel connection of 4 devices, the charge or discharge time is prolonged by 4 times that of a single device since only one fourth of the total current is applied to each single device. Namely, the capacitance is increased by a factor of 4 by connecting 4 devices in parallel. As seen in Fig. 5c and d, the voltage window can be broadened from 0.8 V of a single MSC to 3.2 V of 4 series-connected MSCs. Compared with a single MSC, both capacitance and voltage window double when 4 MSCs are assembled in a combination of series and parallel as indicated in Fig. 5e and f. It should be noted that, like a single MSC, the CV plots of the MSCs assembly also show a quasi rectangular shape and a good symmetry. In addition, the charge and discharge curves of the MSCs assembly are nearly reproducible during cycling, similar to a single MSC. The results justify that the dimension and physicochemical properties are highly consistent for each single MSC, and that screen printing is a facile, practical and scalable technique for the

fabrication of MSCs.

Good flexibility is an indispensable requirement for the practical applications of MSCs in flexible electronic devices. Thus, it is necessary to evaluate the capacitive performance of MSCs under mechanical strain. Accordingly, CV performance of the MSCs was checked at different bending angles as shown in Fig. 6a and b. After being bended at up to 180º, the MSCs exhibit no obvious performance degradation. The durability of the capacitive performance is due to the good adhesion of the active material on Ag electrode and the "adhesive" effect of the gel electrolyte that maintains the integrity of the electrode components. This again confirms that screen printing is a promising method for fabricating flexible MSCs. As a demonstration, a MSCs assembly of 4 series-connected devices can power commercial liquid crystal display (LCD) and light emitting diode (LED) after charging by a 3 V lithium battery as shown in Fig. 6c.

Conclusions

In summary, we fabricated flexible all-solid-state MSCs with a facile screen printing method using N-doped rGO as the active material and PVA/H_3PO_4 as the solid electrolyte. The MSCs show high specific areal capacitance of 3.4 mF cm^{-2} and volumetric energy density of 3.0×10^{-4} Wh cm^{-3}. The screen printed MSCs also exhibit good rate capability and cycling stability with 98.4% capacitance maintained after 2000 cycles. The screen printing method also allows easy scaling up of capacitance and voltage by simply connecting devices in series, parallel or both. This work provides a facile, scalable, cost-effective approach to fabricate MSCs with promising applications as on-chip power sources for micro-devices.

Acknowledgements

This work was supported by the National Basic Research Program of China (2013CB934001), SUTD-ZJU Research Grant ZJURP1100104, the National Natural Science Foundation of China (No. 51101139), and Key Science and Technology Innovation Team of Zhejiang Province under Grant Number 2010R50013.

References

1 A. S. Aricó, P. Bruce, B. Scrosati, J. M. Tarascon and W. V. Schalkwijk, *Nat. Mater.*, 2005, **4**, 366–367.

2 P. Simon and Y. Gogotsi, *Nat. Mater.*, 2008, **7**, 845–854.

3 P. Simon and J. R. Miller, *Science*, 2008, **321**, 651–652.

4 P. Simon and Y. Gogotsi, *Science*, 2011, **334**, 917–918.

5 P. Simon, Y. Gogotsi and B. Dunn, *Science*, 2013, **343**, 1210–1211.

6 M. Kaempgen, C. K. Chan, J. Ma, Y. Cui and G. Gruner, *Nano Lett.*, 2009, **9**, 1872–1876.

7 K. Z. Gao, Z. Q. Shao, J. Li, X. Wang, X. Q. Peng, W. J. Wang and F. J. Wang, *J. Mater. Chem. A*, 2013, **1**, 63–67.

8 X. Xiao, T. Q. Li, P. H. Yang, Y. Gao, H. Y. Jin, W. J. Ni, W. H. Zhan, X. H. Zhang, Y. Z. Cao, J. W. Zhong, L. Gong, W. C. Yen, W. J. Mai, J. Chen, K. F. Huo, Y. L. Chueh, Z. L. Wang and J. Zhou, *ACS Nano*, 2012, **6**, 9200–9206.

9 Z. S. Wu, A. Winter, L. Chen, Y. Sun, A. Turchanin, X. L. Feng and K. Müllen, *Adv. Mater.*, 2012, **24**, 5130–5135.

10 L. Y. Yuan, X. H. Lu, X. Xiao, T. Zhai, J. J. Dai, F. C. Zhang, B. Hu, X. Wang, L. Gong, J. Chen, C. G. Hu, Y. X. Tong, J. Zhou and Z. L. Wang, *ACS Nano*, 2012, **6**, 656–661.

11 J. Xu, Q. F. Wang, X. W. Wang, Q. Y. Xiang, B. Liang, D. Chen and G. Z. Shen, *ACS Nano*, 2013, **7**, 5453–5462.

12 S. Wang, B. Hsia, C. Carraro and R. Maboudian, *J. Mater. Chem. A*, 2014, **2**, 7997–8002.

13 Z. S. Wu, X. L. Feng and H. M. Cheng, *Natl. Sci. Rev.*, 2013, DOI: 10.1093/nsr/nwt003.

14 Y. Wang, Y. M. Shi, C. X. Zhao, J. I. Wong, X. W. Sun and H. Y. Yang, *Nanotechnology*, 2014, **25**, 094010.

15 D. Pech, M. Brunet, H. Durou, P. H. Huang, V. Mochalin, Y. Gogotsi, P. L. Taberna and P. Simon, *Nat. Nanotechnol.*, 2010, **5**, 651–654.

16 D. Pech, M. Brunet, P. L. Taberna, P. Simon, N. Fabre, F. Mesnilgrente, V. Conédéra and H. Durou,

J. Power Sources, 2010, **195**, 1266–1269.

17 G. Y. Zheng, L. B. Hu, H. Wu, X. Xie and Y. Cui, *Energy Environ. Sci.*, 2011, **4**, 3368–3373.

18 P. H. Huang, M. Heon, D. Pech, M. Brunet, P. L. Taberna, Y. Gogotsi, S. Lofland, J. D. Hettinger and P. Simon, *J. Power Sources*, 2013, **225**, 240–244.

19 W. Sun and X. Y. Chen, *J. Power Sources*, 2009, **193**, 924–929.

20 K. Wang, W. J. Zou, B. G. Quan, A. F. Yu, H. P. Wu, P. Jiang and Z. X. Wei, *Adv. Energy Mater.*, 2011, **1**, 1068–1072.

21 M. Q. Xue, Z. Xie, L. S. Zhang, X. L. Ma, X. L. Wu, Y. G. Guo, W. G. Song, Z. B. Li and T. B. Cao, *Nanoscale*, 2011, **3**, 2703–2708.

22 D. Pech, M. Brunet, T. M. Dinh, K. Armstrong, J. Gaudet and D. Guay, *J. Power Sources*, 2013, **230**, 230–235.

23 A. G. Pandolfo and A.F. Hollenkamp, *J. Power Sources*, 2006, **157**, 11–27.

24 L. L. Zhang and X. S. Zhao, *Chem. Soc. Rev.*, 2009, **38**, 2520–2531.

25 Y. P. Zhai, Y. Q. Dou, D. Y. Zhao, P. F. Fulvio, R. T. Mayes and S. Dai, *Adv. Mater.*, 2011, **23** 4828–4850.

26 X. Li and B. Q. Wei, *Nano Energy*, 2013, **2**, 159–173.

27 K. S. Novoselov, A. K. Geim, S. V. Morozov, D. Jiang, Y. Zhang, S. V. Dubonos, I. V. Grigorieva, and A.A. Firsov, *Science*, 2004, **306**, 666–669.

28 M. D. Stoller, S. Park, Y. W. Zhu, J. H. An and R. S. Ruoff, *Nano Lett.*, 2008, **8**, 3498–3502.

29 C. G. Liu, Z. N. Yu, D. Neff, A. Zhamu and B. Z. Jang, *Nano Lett.*, 2010, **10**, 4863–4868.

30 J. J. Yoo, K. Balakrishnan, J. S. Huang, V. Meunier, B. G. Sumpter, A. Srivastava, M. Conway, A. L. M. Reddy, J. Yu, R. Vajtai and P. M. Ajayan, *Nano Lett.*, 2011, **11**, 1423–1427.

31 Y. W. Zhu, S. Murali, M. D. Stoller, K. J. Ganesh, W. W. Cai, P. J. Ferreira, A. Pirkle, R. M. Wallace, K. A. Cychosz, M. Thommes, D. Su, E. A. Stach and R. S. Ruoff, *Science*, 2011, **332**, 1537–1541.

32 S. Park, J. H. An, I. W. Jung, R. D. Piner, S. J. An, X. S. Li, A. Velamakanni and R. S. Ruoff, *Nano Lett.*, 2009, **9**, 1593–1597.

33 C. Lee, X. D. Wei, J. W. Kysar and J. Hone, *Science*, 2008, **321**, 385–388.

34 W. Gao, N. Singh, L. Song, Z. Liu, A. L. M. Reddy, L. J. Ci, R. Vajtai, Q. Zhang, B. Q. Wei and P. M. Ajayan, *Nat. Nanotechnol.*, 2011, **6**, 496–500.

35 M. F. El Kady, V. Strong, S. Dubin and R. B. Kaner, *Science*, 2012, **335**, 1326–1330.

36 M. F. El Kady and R. B. Kaner, *Nat. Commun.*, 2013, **4**, 1475.

37 Q. Zhang, K. Scrafford, M. T. Li, Z. Y. Cao, Z. H. Xia, P. M. Ajayan and B. Q. Wei, *Nano Lett.*, 2014, **14**, 1938–1943.

38 Z. Q. Niu, L. Zhang, L. L. Liu, B. W. Zhu, H. B. Dong and X. D. Chen, *Adv. Mater.*, 2013, **25**, 4035–4042.

39 Z. S. Wu, K. Parvez, X. L. Feng and K. Müllen, *Nat. Commun.*, 2013, **4**, 2487.

40 W. W. Liu, Y. Q. Feng, X. B. Yan, J. T. Chen and Q. J. Xue, *Adv. Funct. Mater.*, 2013, **23**, 4111–4122.

41 W. W. Liu, X. B. Yan, J. T. Chen, Y. Q. Feng and Q. J. Xue, *Nanoscale*, 2013, **5**, 6053–6062.

42 J. L. Xia, F. Chen, J. H. Li and N. J. Tao, *Nat. Nanotechnol.*, 2009, **4**, 505–509.

43 H. B. Feng, R. Cheng, X. Zhao, X. F. Duan and J. H. Li, *Nat. Commun.*, 2013, **4**, 1539.

44 W. S. Hummers and R. E. Offeman, *J. Am. Chem. Soc.*, 1958, **80**, 1339–1339.

45 S. Stankovich, D. A. Dikin, R. D. Piner, K. A. Kohlhaas, A. Kleinhammes, Y. Y. Jia, Y. Wu, S. T. Nguyen and R. S. Ruoff, *Carbon*, 2007, **45**, 1558–1565.

46 Z. H. Sheng, K. Shao, J. J. Chen, W. J. Bao, F. B. Wang and X. H. Xia, *ACS Nano*, 2011, 5, 4350–4358.

47 D. H. Deng, X. L. Pan, L. A. Yu, Y. Cui, Y. P. Jiang, J. Qi, W. X. Li, Q. A. Fu, X. C. Ma, Q. K. Xue, G. Q. Sun and X. H. Bao, *Chem. Mater.*, 2011, **23**, 1188–1193.

48 S. Yang, L. Zhi, K. Tang, X. Feng, J. Maier and K. Müllen, *Adv. Funct. Mater.*, 2012, **22**, 3634–3640.

Figure captions

Fig. 1 (a) SEM image, (b, c) TEM images, and (d) nitrogen EDS mapping of N-doped rGO.

Fig. 2 (a) C1s XPS of GO, (b) C1s and (c) N1s XPS of N-doped rGO, and (d) bonding configuration of N atoms in N-doped rGO.

Fig. 3 Schematic illustration of the fabrication process of flexible all-solid-state MSCs.

Fig. 4 Electrochemical performance of MSCs with N-doped rGO: (a) charge and discharge curves at 20–500 μA cm^{-2}, (b) CV plots at 5–100 mV s^{-1}, (c) charge and discharge curves at 100 μA cm^{-2}, (d) cycling stability at 100 μA cm^{-2}, (e) specific volumetric capacitance at various current densities, and (f) Ragone plot showing the relationship of specific volumetric energy and power.

Fig. 5 Comparison of electrochemical performance of single MSC device and MSCs connected in series and parallel: (a) CV plots and (b) charge and discharge curves of 4 devices connected in parallel, (c) CV plots and (d) charge and discharge curves of 4 devices connected in series, and (e) CV plots and (f) charge and discharge curves of 4 devices connected in a combination of series and parallel. The CV plots are scanned at 50 mV s^{-1} and galvanostatic cycling is performed at 100 μA cm^{-2}. The insets in (a), (c) and (e) are circuit diagrams of the devices.

Fig. 6 (a) Schematic picture of a single MSC bended at different angles, (b) CV plots of the MSC bended at different angles (50 mV s^{-1}), and (c) digital photo of 4 MSCs connected in series that can power commercial LCD and LED after charging by a 3 V lithium battery and the corresponding circuit diagram.

Figures

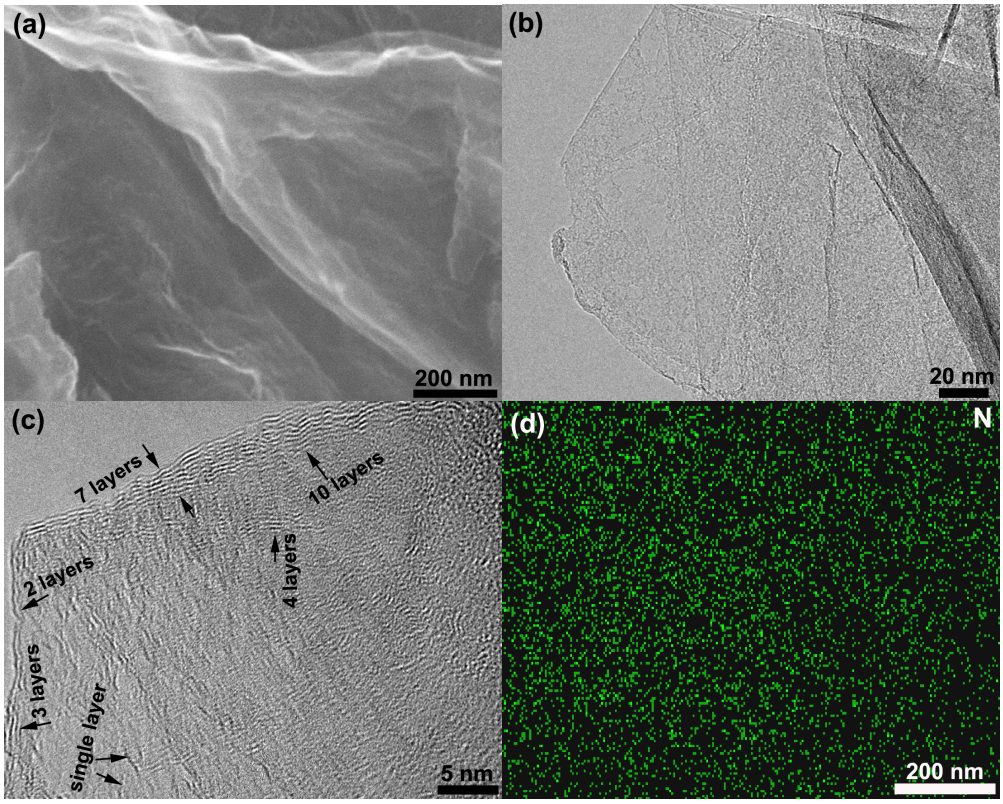

Fig. 1

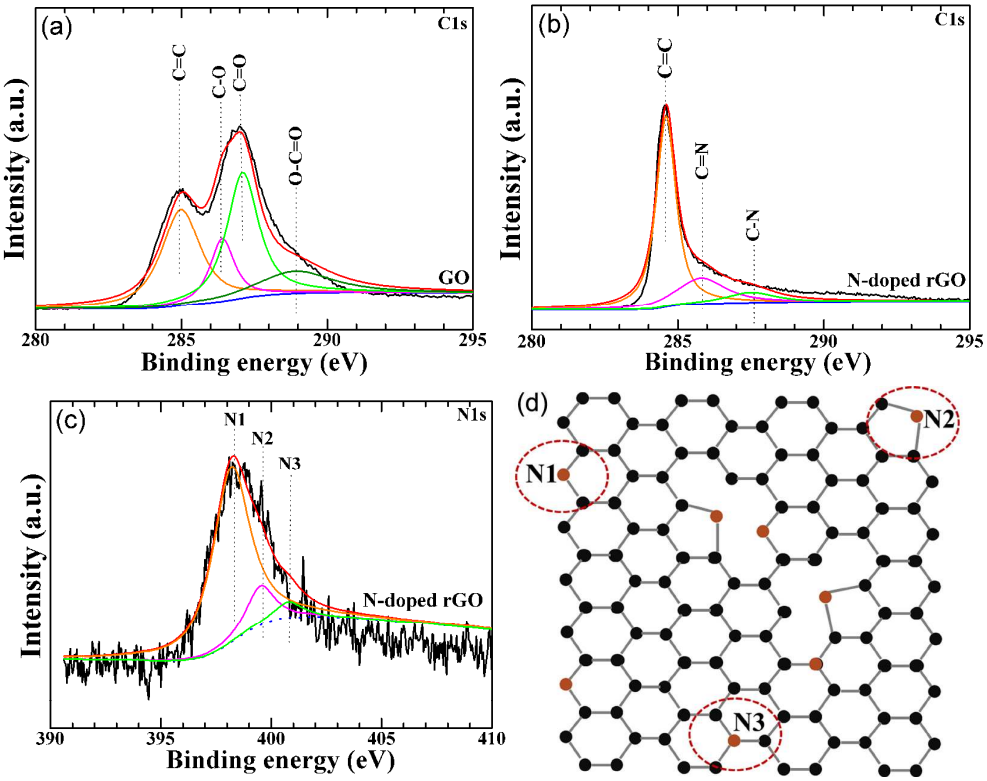

Fig. 2

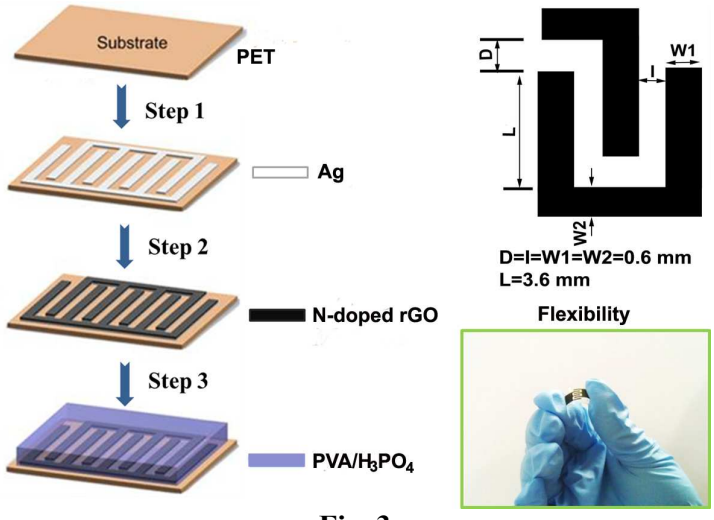

Fig. 3

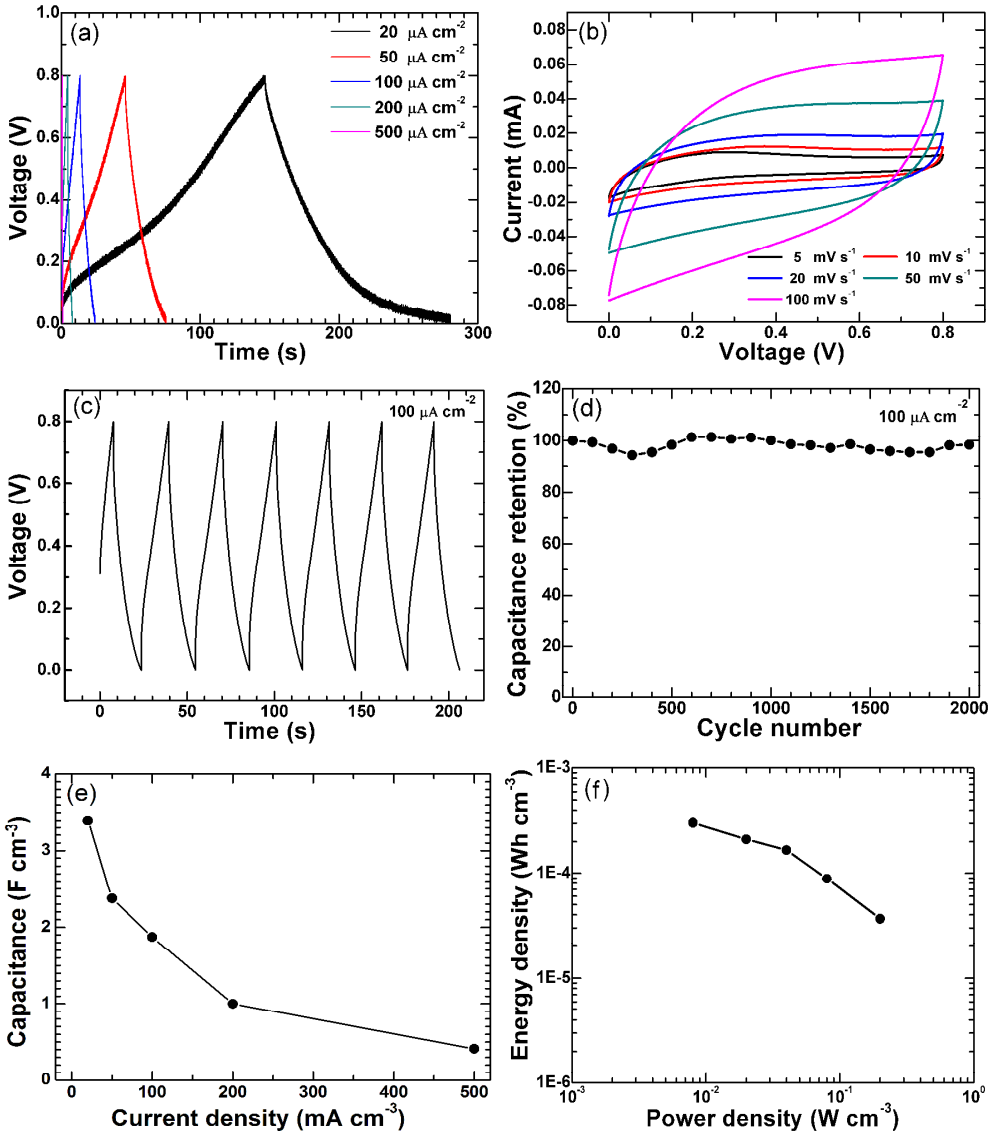

Fig. 4

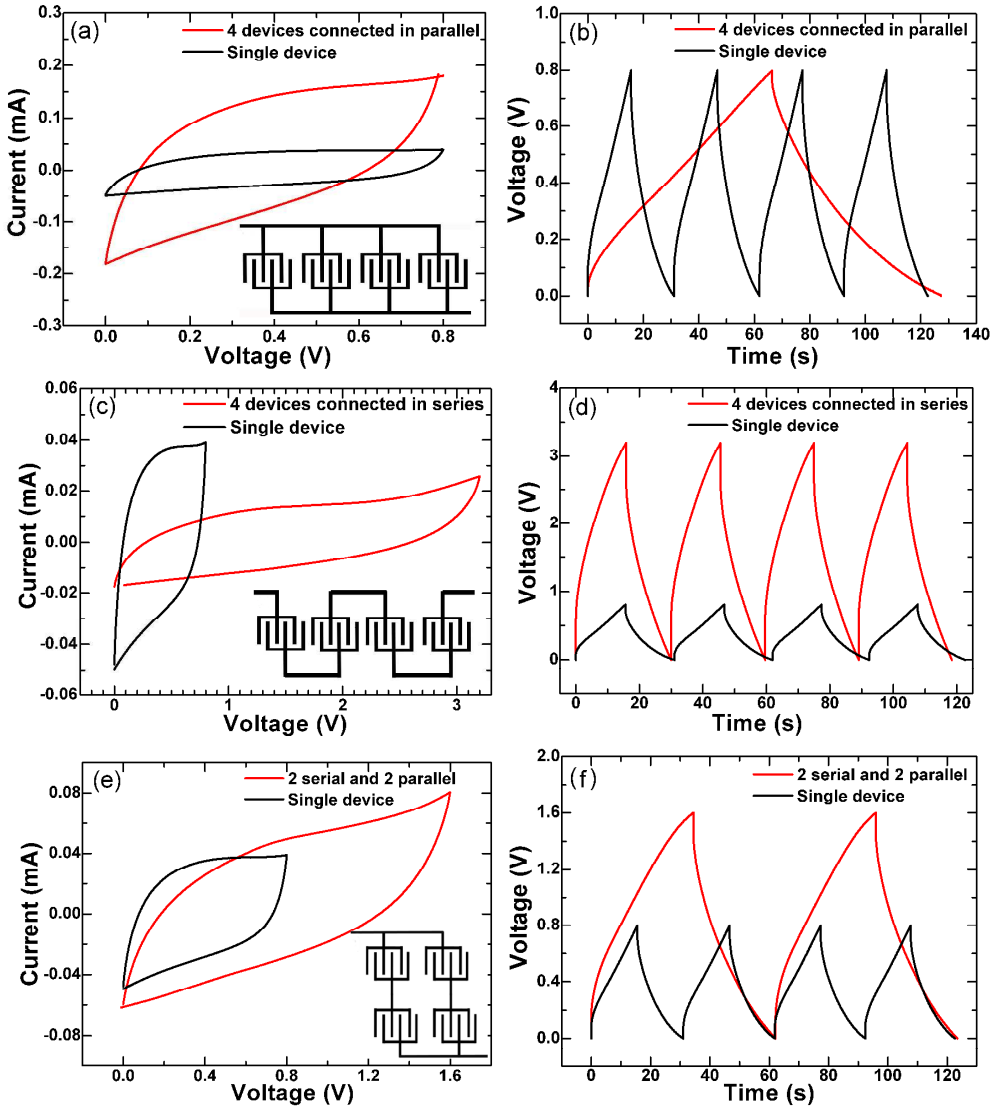

Fig. 5

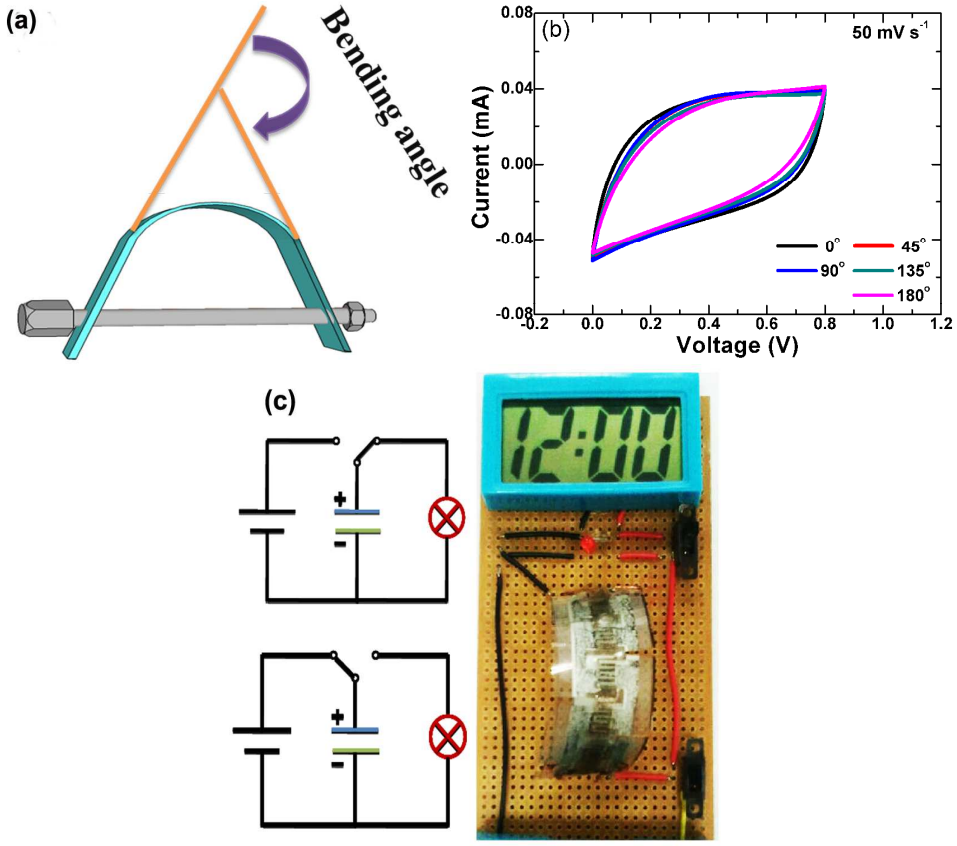

Fig. 6

Table of contents entry

Flexible all-solid-state micro-supercapacitors were fabricated by screen printing method using N-doped reduced graphene oxide as active material and show high specific capacitance and long cycling life.